Wavelength Independent Broadband Directional Couplers in SiN Platform

A THESIS

Submitted by

RIDDHI GOSWAMI – EE19E005

in partial fulfillment of the requirements
for the award of the degree of

BACHELOR OF TECHNOLOGY

DEPARTMENT OF ELECTRICAL ENGINEERING
INDIAN INSTITUTE OF TECHNOLOGY MADRAS.
August 2020

THESIS CERTIFICATE

This is to certify that the thesis titled **Wavelength Independent Broadband Directional Couplers in SiN Platform**, submitted by **Riddhi Goswami**, to the Indian Institute of Technology, Madras, for the award of the degree of **Bachelor of Technology**, is a bonafide record of the research work done by her under our supervision. The contents of this thesis, in full or in parts, have not been submitted to any other Institute or University for the award of any degree or diploma.

Prof. Bijoy Krishna Das
Research Guide
Professor
Dept. of Electrical Engineering
IIT-Madras, 600 036

Place: Chennai, India

Date: Thursday 20th August, 2020

ACKNOWLEDGEMENTS

I would like to take this opportunity to sincerely thank my guide Prof. Bijoy Krishna Das for introducing me to this interesting area of Silicon Photonics. A written acknowledgement is not sufficient to express the sheer magnitude of gratitude I have towards the various people who have given me insight to new opportunities, experiences and also exposure to new information with outmost patience. However, I would like to utilize this opportunity to sincerely thank my guide Prof. Bijoy Krishna Das for kindling and nurturing my interest in Silicon Photonics. In addition to being a great teacher and mentor, he has been a constant source of encouragement, support and guidance.

I would also like to thank the entire Integrated Optoelectronics Group for being the most helpful seniors, and for helping me out with my problems.

I would also like to thank my friends for being there when it mattered, for cheering me up in my lows and helping me get through this entire conundrum. I would also like to thank my batch-mates and fellow exchange students for making this experience memorable.

Finally, I would like to thank my parents and my little sister for supporting in me in all my endeavors, for taking the good with the bad and for tolerating all my tantrums. I will forever be grateful to God for the beautiful family I have been blessed with.

ABSTRACT

Integrated silicon photonics technology has revolutionized short-haul data communication by replacing bandwidth limited metal interconnects with high-speed optical interconnects. Micro-ring resonators (MRRs) and Mach-Zehnder interferometers (MZIs) are the two most important building blocks of an integrated photonics chip. Their functionality lies in a wide range of applications such as spectral filters and switches, sensing, modulation, photon pair generation, RF filters, etc. Conventionally, both MRR and MZI structures are constructed with suitably designed directional couplers. In general, silicon photonic DCs are highly wavelength dependent. This eventually limits the optical bandwidth of an integrated optical circuit designed with MRRs and MZIs. Thus there is a need for designing DCs with scalable power splitting ratios, operating uniformly over a broad wavelength range . In silicon nanostructures, challenges also remain in reducing their linear and nonlinear losses . Recently SiN is gaining popularity due to its low-loss and chip-scale solutions that benefit from transparency over a wide wavelength range (400–2350 nm) as a complimentary platform to silicon-on-insulator (SOI) .Also device characteristics in SiN are found to be much more tolerant to width variations due to fabrication. Here we demonstrate the potential of silicon nitride (Si_3N_4) platform by realizing compact, wavelength independent low-loss directional couplers on it.

In this thesis work, we have studied the wavelength dependent coupling characteristics of DCs consisting of two single-mode rib waveguides as a function of waveguide width (W), slab height (h) between the coupled waveguides in silicon nitride-on- insulator substrate with a device layer thickness (H) of 450 and 500 nm in each case for varying widths. The reason for choosing this thickness is for suitable integration with grating couplers which are found to work better in this range. Solving the two lower order eigenmodes (supermodes) of a symmetric DC (constructed with two identical single-mode waveguides), we investigated their dispersion characteristics. In order to achieve a wavelength independent coupling, one needs to match the group indices of guided super-modes in DC. To design such a DC, we first calculated the wavelength dependent differential group index $\Delta n_g(\lambda)$ of supermodes by varying the cross-section design parameters. By analyzing the simulation results, a wavelength independent (WIDC)

geometry is optimized offering uniform coupling over 1425 nm≤ λ ≤ 1725 nm in SiN.

A set of WIDCs with various power splitting ratios were realized by changing the coupling length. This is an entirely simulation based report. All the simulations were carried out following boundary conditions in *finite difference eigen-mode solver* (FDE) of Lumerical MODE Solutions [29] .

After successful demonstration of WIDC based power splitters in SiN platform, we can further extend the work towards the implementation of broadband MRRs and MZIs in TE-polarization on the same platform in future.

TABLE OF CONTENTS

LIST OF FIGURES

ABBREVIATIONS

Acronyms

BOX	Buried Oxide
CMOS	Complementary Metal Oxide Semiconductor
DC	Directional Coupler
EBL	Electron Beam Lithography
ER	Extinction Ratio
FSR	Free Spectral Range
MZI	Mach-Zehnder Interferometer
MMI	Multi-Mode Interference
MRR	Microring Resonator
MZI	Mach-Zehder Interferometer
SMF	Single Mode Fiber
SOI	Silicon-on-Insulator
SiN	Silicon Nitride
SR	Splitting Ratio
SWG	Sub-Wavelength Grating
TE	Transverse Electric (polarization)
TM	Transverse Magnetic (polarization)
WDM	Wavelength Division Multiplexing
WIDC	Wavelength Independent Directional Coupler

Units

dB	decibel
dBm	decibel milli-watt
nm	nanometer
ns	nanosecond
K	Kelvin
μm	micrometer
μs	microsecond

NOTATIONS

n	Refractive index
$\mathbf{n}_{eff}$	Effective refractive index
$\boldsymbol{s}$	Permitivity
$\boldsymbol{\lambda}$	Wavelength
$\boldsymbol{\beta}$	Propagation constant
$\boldsymbol{\varphi}$	Phase of the EM wave
L	Length (refers to device length, component length)
$\boldsymbol{\Gamma}$	Confinement factor
$\boldsymbol{\alpha}$	Loss per unit length
$\boldsymbol{\kappa}$	Coupling coefficient

CHAPTER 1

1. Introduction

Wavelength dependent performance of a typical directional coupler (DC) limits the optical bandwidth of important silicon photonics components like Micro-ring resonator (MRR) and Mach-Zehnder interferometer (MZI) which find their applications in important fields such as bio-sensing, modulation, filter, switches, photon-pair generation , etc. SiN offers more flexibility in terms of fabrication tolerance and losses compared to SOI. The benefits and disadvantages of the platform are listed in this chapter along with the motivation for utilising SiN as a complementary platform. Within the scope of this work, we theoretically investigated coupling characteristics of a DC comprised of two single mode waveguides in silicon nitride-on-insulator platform and conditions for wavelength independent operation, followed by the design of a wavelength independent DC (WIDC) operating uniformly over a broad wavelength range of approximately 300-nm near $\lambda = 1550$ nm in TE polarization. Broadband WIDCs with various power splitting ratios were demonstrated. The outcome of these results can be further extended towards the demonstration of Micro-ring resonators (MRRs) and Mach-Zehnder interferometers (MZIs). Such devices are highly desired for broadband wavelength division multiplexing (WDM), reconfigurable signal switching/routing, add/drop filters, and many more applications. The research motivation including literature review, set of objectives, advantages and thesis organization have been presented in the following sections.

1.1 Motivation

Optical interconnects are being used in recent times to overcome the fundamental bandwidth bottleneck of metallic interconnects in VLSI electronic chips. An optical interconnect by virtue of its higher carrier frequency offers higher data rate, lower

latency, and lower power consumption, etc [1]. Due to its transparency in the range of optical wavelengths and CMOS compatibility, Silicon is used to make these optical interconnects. A major driving factor to deviate from SOI is the desire to operate in spectral bands where silicon or silicon oxide are absorbing.

Here we state our major reasons for the popularity of SiN platform:-

1. *Transparency range*: SOI-based waveguides have low absorption losses from 1.1 μm to about 3.7 μm while SiN is transparent throughout most of the visible range – down to at least 500 nm .
2. *Index contrast*: Very high index contrast allows one to have a very compact footprint but at the same time it makes the waveguide prone to scattering losses due to sidewall roughness. It also implies high sensitivity of the effective index to the waveguide width [2] and therefore less fabrication tolerance. The lower index contrast of the SiN system is a boon in this case.
3. *Low loss*: SOI-based strip waveguides completely surrounded by a silica cladding have typical waveguide losses of 1 to 2 dB/cm, largely due to the scattering associated with sidewall roughness. In SiN photonic wires these losses can in principle be an order of magnitude lower [3].
4. *Third order nonlinearity*: The Kerr nonlinearity of silicon is huge but unfortunately in the 1300/1550 telecom bands, suffers from huge losses because of two-photon absorption (TPA) especially at high powers. Silicon nitride has a weaker Kerr nonlinearity but the TPA is virtually zero in view of the material's large band gap [4]. Therefore it has been possible to demonstrate frequency comb generation as well as super continuum generation in SiN photonic wires [5,6]. Thus a distinguishing advantage of SiN is its wide bandgap with no two-photon absorption for wavelengths above 800 nm.
5. *Second order nonlinearity and Pockel's effect*: In principle both silicon and silicon nitride have negligible second order nonlinearity and Pockels effect in view of the centro-symmetry of both materials .Such nonlinear effects would be highly desirable for creation of efficient electro-optic modulators. In SOI-case one can resort to free carrier induced electro-refraction

(making use of first order non-linearity effects), but resulting modulators have a large footprint and consume a lot of power at high modulation speed. Active elements are difficult to realize in SiO2 or SiN due to difficulty in tuning the refractive index of the host material. But in recent years strong electro-refraction has been reported in SOI waveguides in which a strain gradient was induced by means of a strained silicon nitride over-layer. The precise mechanism for this phenomenon is still a matter of debate, but one recent report attributes the effect to a strain gradient in the silicon nitride rather than that in the silicon [7]. This may open the door to novel strained SiN-based Pockels-modulators.

A number of very recent works have started to demonstrate the unique potential of SiN. Since the Q-factors of SiN micro-resonators are not yet material absorption limited [8], further refinement of the fabrication techniques promises even higher Q's for integrated quantum optics [9,10]. Finally, the broad transparency of SiN combined with low loss and excellent dispersion engineering makes it a very flexible platform and a promising technology for future applications.

Alternatively, InP is also used in many standalone PIC applications and as a gain block for SOI PICs with a tradeoff in higher waveguide losses and larger bend radii, as compared to SOI; with very limited transparency window to be any useful for broadband operation [3].

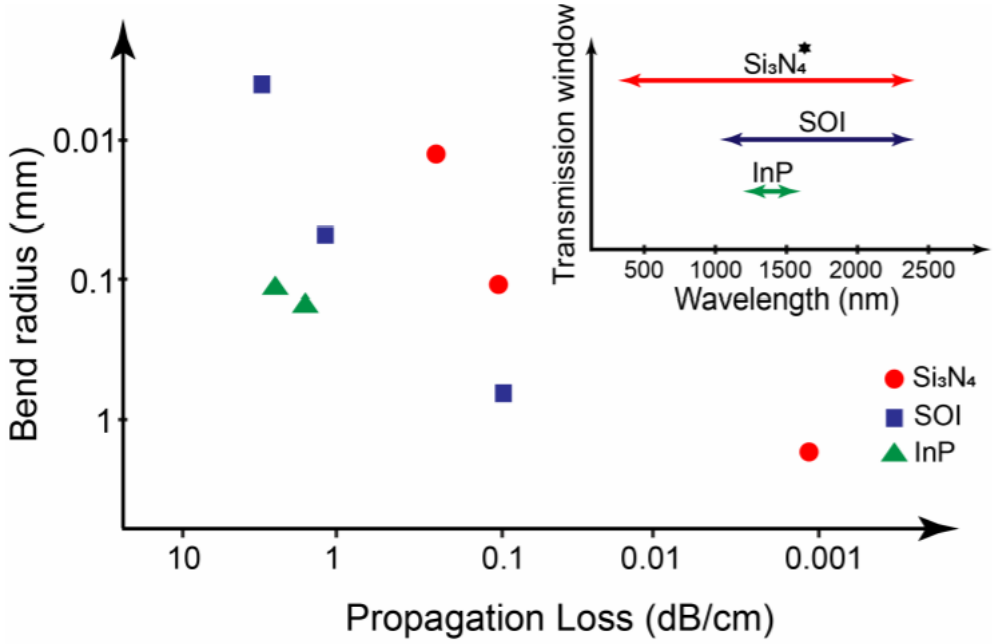

Figure 1.1: Bend radii, propagation loss, and window of transparency for published Si3N4, SOI, and InP waveguides [3]

MRR [13] and MZI [16] are the basic building blocks of many silicon photonics applications. Both MRR and MZI structures are mostly constructed with suitably designed multimode-interferometers (MMIs) or directional couplers (DCs). In comparison with MMIs, DCs are more superior in-terms of coupling efficiency, scalability and easiness of fabrication .In this thesis we focus on 2×2 DCs designed with two single mode waveguides in silicon nitride over insulator. In the following section we briefly discuss about the basic DC-based switch cell configurations and their switching characteristics affected by wavelength dependent DC operation.

1.1.1 Bandwidth Limitation of DC: Examples

Schematic representation of a typical add-drop MRR based switch cell is shown in Fig 1.2(a). Input wavelengths which are resonant to the ring appear at the drop port while those non-resonant appear at the through port. An integrated micro-heater is used to tune the transfer function between the output ports. Figure1.2(b) shows the schematic of

ideal transfer function at the through port for "off" state and "on" state of the switch. The spectrum shows uniform extinction for all operating wavelengths. However in practice extinction is not uniform as coupling coefficient involved is wavelength dependent. Thus the effective optical bandwidth of a MRR is limited.

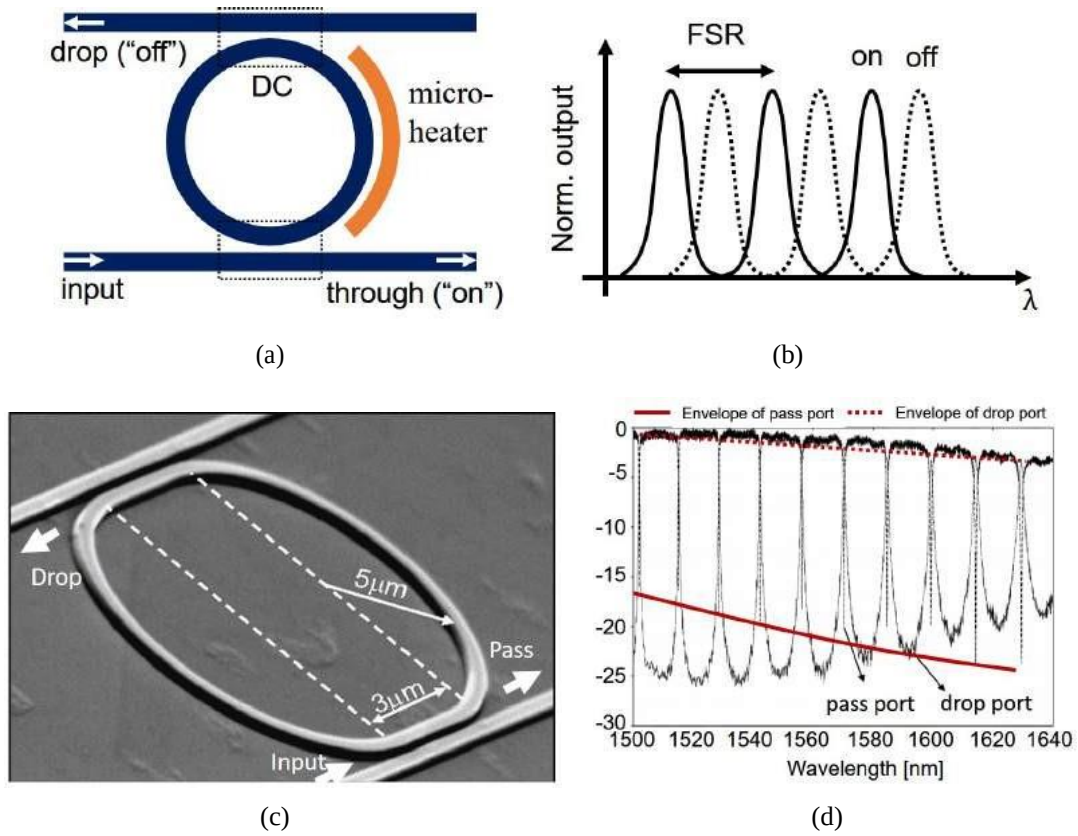

Figure 1.2: (a) Schematic of an add-drop MRR based switch cell and the corresponding ideal switching characteristics at the through port in (b). (c) SEM image of a fabricated add-drop MRR and (d) the corresponding transmission characteristics measured at the through- and drop- ports [14].

A fabricated MRR based add-drop multiplexer and its typical transmission characteristics are shown in Fig ure1.2(d). It is evident that both the spectra have non-uniform extinction ratio (ER) over the entire range of wavelength (highlighted with red lines).

This is because of the wavelength dependent coupling characteristics of DCs used. A similar pattern of non-uniform response is also observed in MZIs due to wavelength dependent response of the DCs involved.

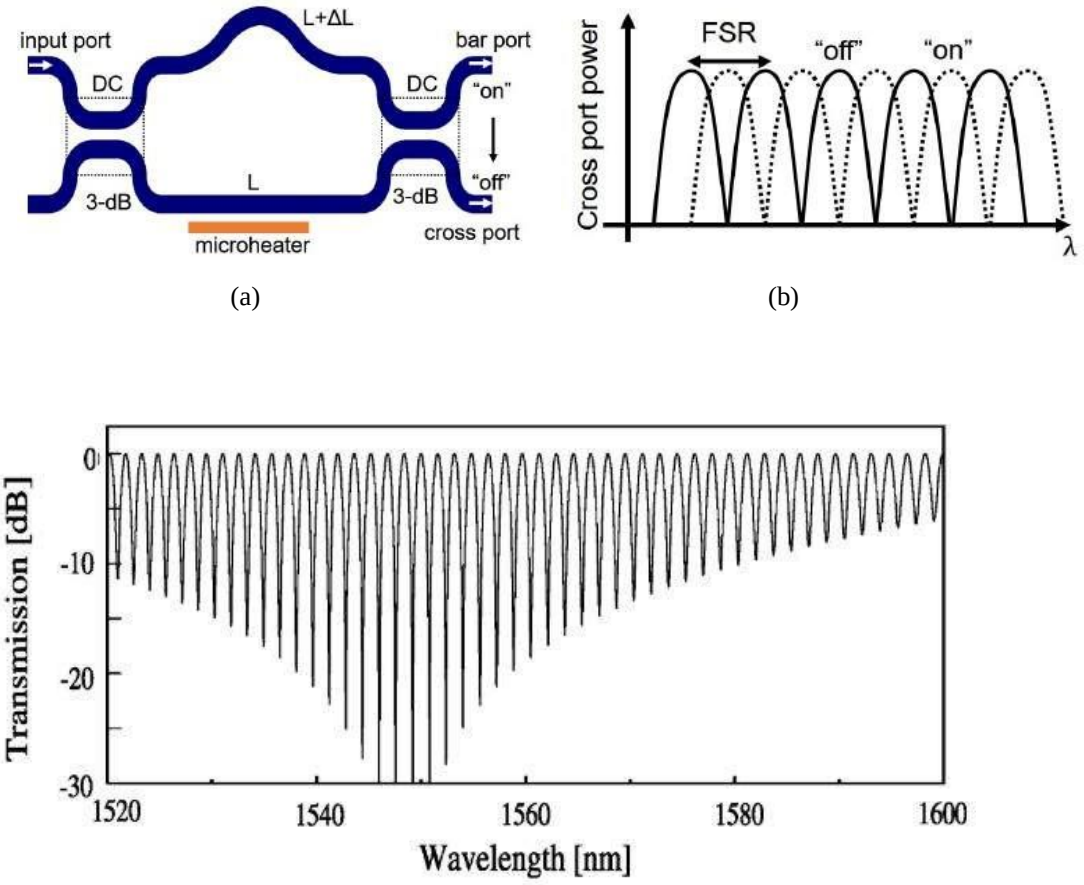

Figure 1.3: (a) Schematic of a 2 ×2 unbalanced MZI-based switch and (b) the transmission characteristics at Port 4 for "on" and "off" state of the switch (ideal case). (c) Actual wavelength dependent transmission characteristics calculated at Port 3. Waveguide parameters: width = 500 nm, height = 220 nm, gap of DC = 2.5 μm, effective L_{DC} = 6.8 μm, ΔL = 393.6 μm [15].

.

Typical 3D layout of a conventional 2×2 DC (power splitter) is shown in Figure1.4(a), consisting of two single mode waveguides mutually coupled through their evanescent fields. Since the waveguide dimensions (W - width, H - height) and the separation (G - Gap) are in sub-wavelength range , the coupling characteristics of a DC is strongly depends on the operating wavelength ($\lambda \sim 1550$ nm) [17].

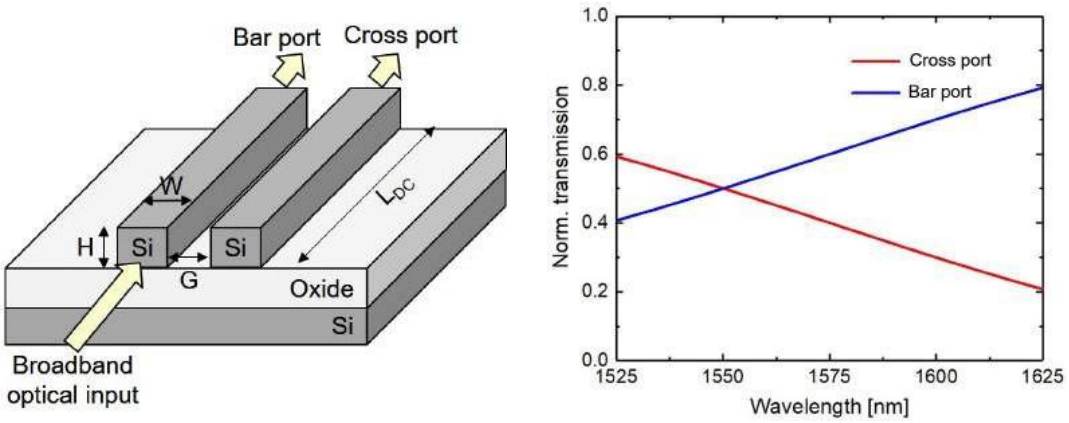

(a) (b)

Figure 1.4: (a) Typical 3D scheme of a SOI DC with two parallel coupled waveguides (W - width, H - height, G - Gap and L_{DC} - DC length) in SOI; (b) power splitting ratio at the bar port and cross port of a 3-dB DC ($L_{DC} = L_{3dB}$) designed at $\lambda = 1550$ nm corresponding to a broadband optical input (1525 nm$<\lambda<$1625 nm) [17].

Typical wavelength dependent power splitting ratio at of a conventional DC designed for 3-dB power splitting at $\lambda = 1550$ nm are shown in Figure1.4(b). This clearly indicates that the optical bandwidth of a SOI DC is limited by the wavelength dependent coupling between the waveguides. This eventually limits the optical bandwidth of an integrated optical circuit designed with MRRs and MZIs . A detailed working principle of DC is given in Chapter 2.

1.1.2 Broadband DCs : Design Approaches

In recent years, various design approaches have been reported to enhance the bandwidth of DCs. In this section we briefly review some of the relevant efforts.

Approach - 1: Unbalanced MZI based structures [24,25,26] with low contrast waveguides. A schematic of a MZI based wavelength insensitive coupler is shown in Figure1.5. The basic idea is to introduce an additional phase delay $\Delta\varphi$ in one of the arms which compensates the wavelength dependent phase in the DCs. However, this design is not suitable for scalable power splitting ratio, since it requires adequate control over k_1, k_2 and ΔL and also it increases footprint.

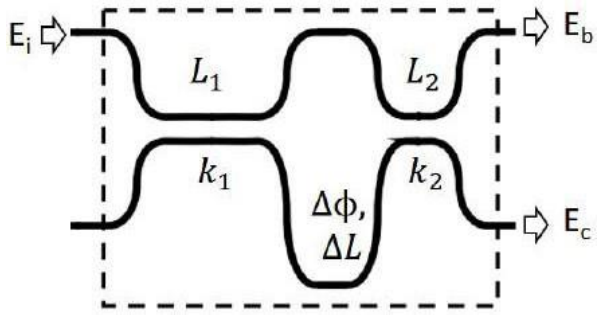

Figure 1.5: Scheme of a wavelength insensitive coupler proposed in [19].

Approach - 2: Lu *et al.* proposed and demonstrated broadband DCs separately for TE and TM polarizations, using asymmetric-waveguide based phase control [21] (see Figure1.6). The cross-sectional view of the symmetric coupler and asymmetric phase control sections are shown in Figure1.6 . Here, wavelength dependent phase in the symmetric couplers are compensated by a small phase difference between the two waveguides in the phase control section. The phase control section is comprised of two asymmetric waveguides and separated by relatively wider gap .However; these broadband power splitters require critical waveguide parameters. Also the presence of asymmetry in the coupler make the device less stable against temperature fluctuations.

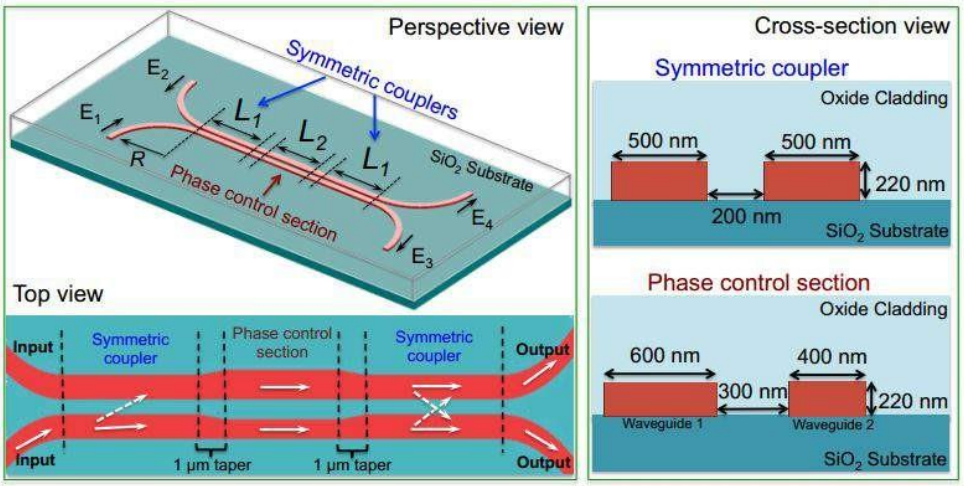

(a)

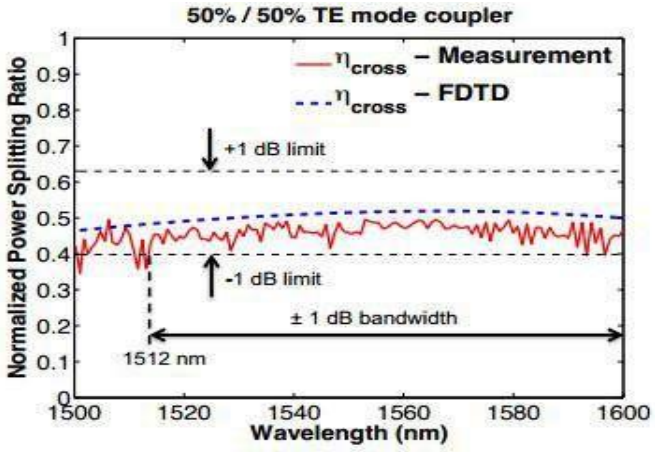

(b)

Figure 1.6: Scheme of a broadband silicon photonic directional coupler using asymmetric-waveguide based phase control [21].

Approach - 3: An alternate method to enhance the bandwidth of DC is the direct integration of sub-wavelength gratings (SWGs) in the coupling region of DC as proposed by Hailir in Ref [22] (Figure1.7(a)). Sub-wavelength gratings (SWG) can be used to engineer the dispersion of directional coupler supermodes, and thus increase operational bandwidth. However, SWG directional couplers are sensitive to grating pitch and fill-factor variations, and it may be challenging to meet the required minimum feature size. In this case, SWG embedded DC, the index perturbation in the coupling region changes the slope of the effective index of the fundamental (φ1) mode while that of first order (φ2) mode of DC is unaffected (due to its lobes that balance out the change). This reduces the wavelength dependency in the power coupling

strength between the waveguides. The transmission characteristics of a demonstrated 3-dB power coupler based on SWG DC [23] is shown in Figure1.7(b). The device exhibits nearly 100 nm bandwidth. However, they require adequate control over design parameters of SWGs (period, duty cycle, width, extension length of gratings to both sides of DC, etc.) and DC (waveguide width, gap, etch depth, etc).

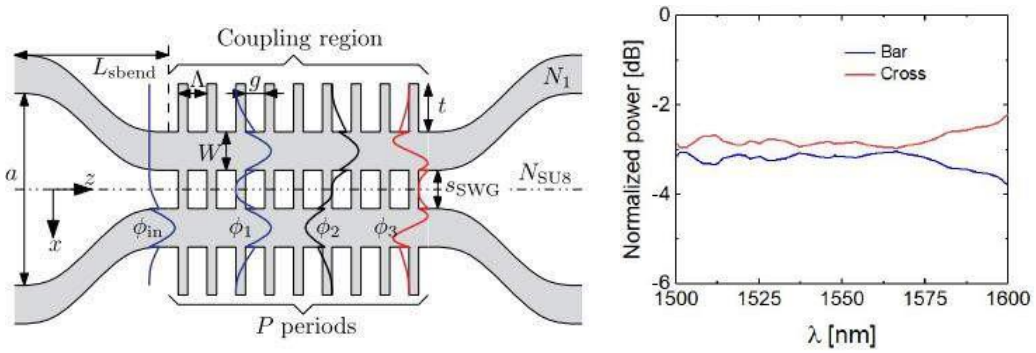

(a) (b)

Figure 1.7: (a) Proposed scheme of a broadband directional coupler with dispersion engineered sub-wavelength structures [22]; (b) normalized optical powers for a fabricated SWG DC demonstrated in [23].

More compact 3-dB power splitters are also reported with curved symmetric directional coupler [24,25] and hybrid plasmonic waveguides[26,27]. To conclude, all the above discussed approaches require extra design parameters to be controlled accurately for any decisive performances. Moreover, it appears not so easy task to design a DC with scalable power splitting ratio using these approaches. Thus there was need for a simple DC design for scalable power splitting and operating over a broad wavelength range for large-scale integrated photonic switching circuits that simply depends on device dimension .

1.2 Research Objective

With the view of above mentioned limitations, the objective of this thesis was set to investigate the design a compact DC in nitride platform operating uniformly over a

wider wavelength range such that power splitting ratio could be scaled by simply varying the device length(coupling length). The best possible design of a DC (with the broadest possible optical bandwidth) could then be used to demonstrate wavelength independent MRRs and MZIs in future works.

1.3 Thesis Organization

The rest of this thesis is organized with the description of design aspects of various DCs with different dimensions, important results and their analyses. They are discussed chapter-wise as follows:

In chapter 2, we have discussed about the design and demonstration of WIDCs with scalable power splitting ratios. We started with theoretical understanding of polarization dependent single-mode waveguide design followed by studying the waveguide dispersion characteristics using numerical simulations. A condition for wavelength independent coupling has been established by solving the guided super-modes of a DC [28].

Also , we have presented the design and demonstration of broadband of wavelength dependent DC on nitride platform with optimized device dimensions for wavelength independent operation.

A summary of the research carried out within the scope of this thesis and possible extensions of the work have been briefly outlined in Chapter 3

CHAPTER 2

2. Directional Coupler: Design and Demonstration

In this chapter we have studied the coupling characteristics of a conventional 2×2 DC structure towards the design and demonstration of wavelength independent DC (WIDC) operating near λ=1550 nm. Typical layout of a 2×2 DC is shown in Figure 2.1(a)(*x*-*z* plane). The cross and bar-ports are indicated with respect to one of the input ports. The two waveguides are assumed to be identical and separated by a small gap *G* over a coupling length (along *z*-axis) of L_{DC} as shown.

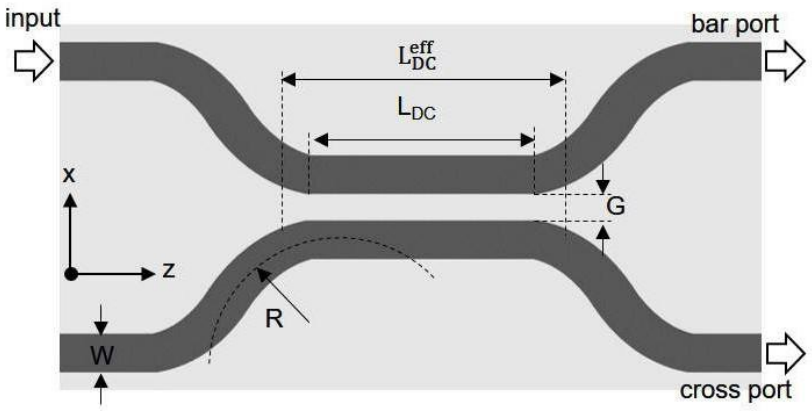

(a)

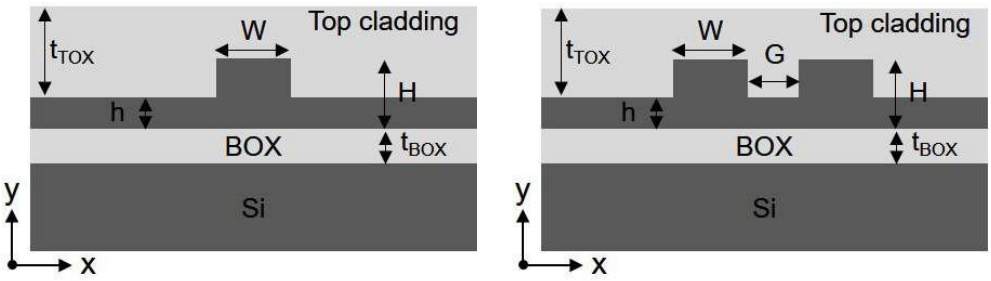

(b) (c)

Figure 2.1: (a) Top view of a 2x2 DC, (b) and (c) are cross-sectional views of input/output waveguide and DC respectively in SOI substrate. L_{DC}: DC length, *W* : rib width, *h*: slab height, *G*: gap, *H*: device layer (rib) height and *R*: waveguide bend radius, t_{BOX}: buried oxide thickness and t_{BOX}: top oxide thickness.

However, the effective the coupling length of DC must be longer than L_{DC}, to accommodate for additional losses in the bent coupling section. A sharper S-bends (or a smaller R) may be desired for compact device footprint as well as to limit couplings in the bend regions. The gap G controls the mode overlap and coupling strength of DC for any fixed waveguide geometry. A cross-sectional view (in x-y plane) of individual waveguides and DC region in SOI substrate along with important design parameters are shown in Figures 2.1(b) and 2.1(c), respectively. The waveguide geometry is defined by rib width W , height H and slab height h. Following the standards of silicon photonic foundries, we have considered a 220-nm thick device layer (H) SOI substrate with buried oxide layer (SiO_2) thickness (t_{BOX}) of 2 μm and handle silicon layer of thickness of 500 μm. The Silicon would be etched out and Silicon Nitride deposited to check the benefits of alternative platform in case of actual fabrication. The waveguides may be assumed to be covered with a top cladding layer of air/oxide.

With suitable choice of design parameters it is possible to engineer the dispersion characteristics of waveguides and hence the DC design towards wavelength independent operation over a given wavelength range. Moreover nitride platform is less dispersive owing to lower index contrast and therefore offers better wavelength independent characteristics but device footprint is more here.

In following sections we have looked into the wavelength dependent coupling characteristics of coupled single-mode waveguides from simulation results.

2.1 Waveguide Design

Light is confined both vertically and horizontally in the core region (x-y plane) in 2D rib waveguides. The index contrast increases with etch depth (d = H − h), but the rough sidewalls increase the propagation loss due to sidewall scattering. In our theoretical discussions, we have considered loss-less waveguides with smooth and vertical sidewalls. In general, waveguides are designed for single-mode operation except for some application .In other words the phase velocity difference between the guided modes cause inter-modal dispersion in multi-mode waveguides.

However, in single-mode waveguides due to the tighter confinement of modes in submicron waveguides, the effective index (n_{eff}) of guided mode varies significantly with wavelength. This is called intra-modal (structural) dispersion, resulting in wavelength dependent group index, ($n_{g(\lambda)}$). Therefore, it is important to estimate the valid range of W and h (fixed H) and their polarizations for single-mode guidance over a desired wavelength range .

2.1.1 Single-Mode Guidance

At any operating wavelength λ, the number of guided modes and their polarizations are decided by waveguide geometry (W , h and H). The polarization of supporting modes inside the waveguide can be ether TE-like (dominant electric field component parallel to the substrate) or TM-like (dominant electric field component perpendicular to the substrate).The possible supporting modes of a waveguide of certain geometry are calculated by solving the Maxwell's equation with appropriate boundary conditions. Commercial *finite difference eigen-mode solver* (FDE) of Lumerical MODE Solutions [29] is used to calculate the geometry dependent effective index (n_{eff}) , wavelength dependent group index, ($n_{g(\lambda)}$) and polarization fraction of m^{th} ($m = 0, 1$) order guided mode for various W (500 nm ≤ W ≤ 1200 nm) and h (0 ≤ h ≤ 500 nm) at an operating wavelength $\lambda = 1550$ nm. The degree of polarization of the guided modes are defined by comparing the fraction of transverse electric field component along x-direction:

$$\gamma_x = \frac{\int |E_x|^2 dxdy}{\int (|E_x|^2 + E_y{}^2) dxdy} \qquad (2.1)$$

where, E_x and E_y are the transverse electric field components of a guided mode. For convenience, we have assumed a guided mode to be TE-polarized if $\gamma_x \geq 0.6$ [28]. Besides single-mode guiding condition, we also made sure from individual simulation of each DC that TE_0 mode is supported for each DC.

The following figure shows TE and TM polarizations in a SiN waveguide.

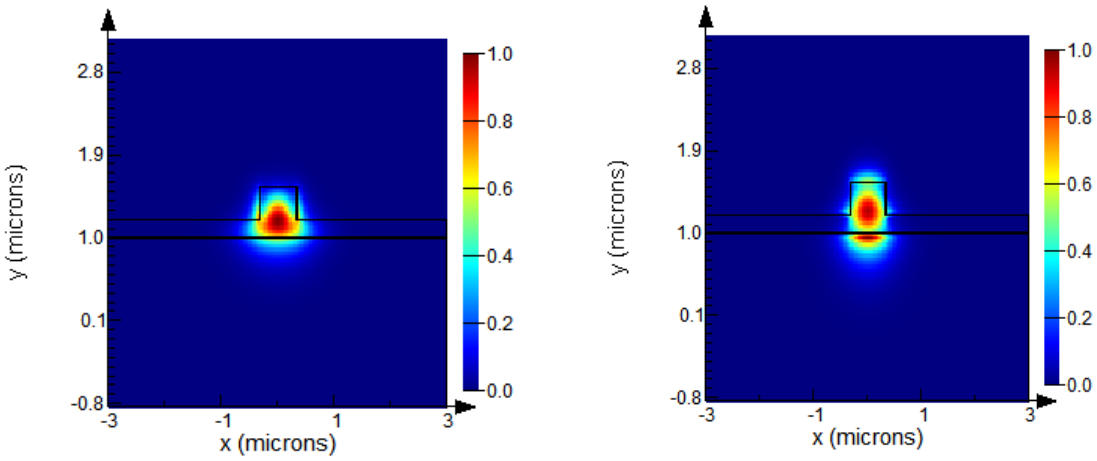

(a) (b)

Figure 2.2: Electric field intensity distribution of (a) TE_0 and (b) TM_0 modes of a SiN waveguide of W = 650 nm, h = 200 nm and H = 450 nm calculated at λ = 1550 nm with air cladding .

2.1.2 Modal Dispersion

The n_{eff} of a waveguide is not only a function of waveguide geometry but also a function of wavelength. The wavelength dependent effective index of a guided mode results in structural dispersion. To calculate the $n_{eff}(\lambda)$, the material dispersion parameters of Si, SiN and SiO_2 given in [30] in Lumerical MODE Solutions for 1425 nm $\leq \lambda \leq$ 1725 nm were included. Note that, irrespective of the waveguide geometry and cladding, n_{eff} reduces as wavelength increases. Moreover, n_{eff} is a strong function of λ for smaller core area waveguides . Thus deeply etched waveguides are highly dispersive than shallow etched waveguides.

In submicron waveguides, the modal confinement and evanescent field distributions are also strong functions of wavelength. Since the effective index reduces with wavelength , the evanescent tail penetrates more into the slab region and hence power confined within the core reduces with wavelength. Deeply etched waveguides confine more light in the waveguide core due to higher refractive index contrast. On the other hand, confinement increases with core size for shallow etched rib waveguides. The modal confinement reduces with oxide cladding since the refractive index contrast is more with air cladding. However confinement is less in SiN due to lower index contrast of the nitride platform compared to SOI. Lower confinement increases the bend induced losses and hence limits the bending radii of the s-bends. As a result we need larger bending radii for devices in SiN platform

2.2 Dispersion in Coupled Waveguides

To understand the dispersion in coupled waveguides we first discuss the working principle of a DC and thereafter the wavelength dependent propagation of its guided eigen modes (supermodes).

2.2.1 Coupled Waveguides: Working Principle

The coupling characteristics of a 2×2 DC can be explained using supermode analysis [31]. Figure2.3(a) shows two single-mode waveguides with field amplitudes $E_1(x, y, z)$ and $E_2(x, y, z)$ propagating along $z-$ direction with propagation constants $\beta_1 = 2\pi n_{eff1}/\lambda$ and $\beta_2 = 2\pi n_{eff2}/\lambda$, respectively. The gap (G) is such that their field amplitudes are non-overlapping and hence waveguides are uncoupled. Whereas in case a of coupled waveguide system, as shown in Figure2.3(b), the evanescent tails of the two guided modes can overlap in the small gap. If the two single-mode waveguides are identical, one can expect two lowest supermodes (symmetric supermode and antisymmetric supermode) which are the linear combination of the individual uncoupled waveguide modes E_1 and E_2.

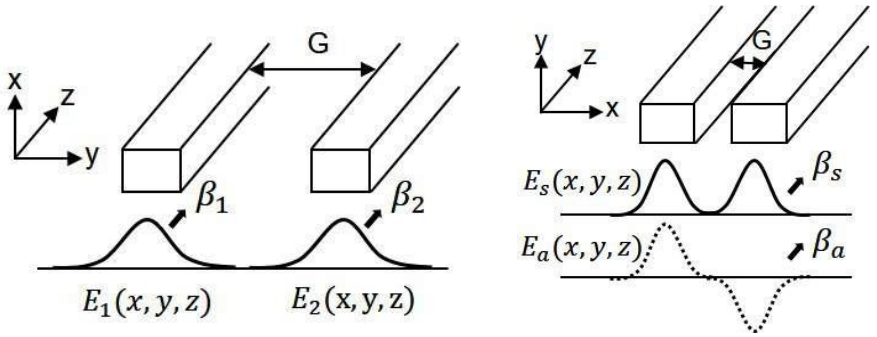

(a) (b)

Figure 2.3: Schematics of (a) uncoupled waveguides and (b) directional coupler (DC); $E_1(x, y, z)$ and $E_2(x, y, z)$ are the electric field distributions of individual waveguides; $E_s(x, y, z)$ and $E_a(x, y, z)$ are the electric field distributions of two lowest order modes (symmetric & antisymmetric supermodes) of a DC

$$E_s(x, y, z) = E_s(x,y) \exp(j\beta_s z) \quad (2.2a)$$

$$E_a(x, y, z) = E_a(x, y) \exp(j\beta_a z) \quad (2.2b)$$

Where E_s and E_a are the cross-sectional electric field profiles of the symmetric supermode (or fundamental mode) and antisymmetric supermode (or first order mode) respectively. The propagation constants β_s and β_a of the two modes are given by:

$$\beta_s = \frac{2\pi}{\lambda} n_{eff}^{s}(\lambda) \quad (2.3)$$

$$\beta_a = \frac{2\pi}{\lambda} n_{eff}^{a}(\lambda) \quad (2.4)$$

where n_{eff}^{s} and n_{eff}^{a} are the effective indices of symmetric and anti-symmetric super-modes respectively. Since $n_{eff}^{a} < n_{eff}^{s}$, both modes travel with different velocities and hence *their relative phase difference ($\varphi = (\beta_s - \beta_a)z$) decides the fraction of power coupled from one waveguide to other waveguide* at any distance along the coupled region. Here we assume that the two waveguides are identical such that $\beta_1 = \beta_2$ and lossless propagation. Lc is defined as the cross-coupling length (interaction length of DC required for the complete exchange of power from one waveguide to other).

In general, the amplitude transfer functions of a 2×2 DC can be expressed as [32]:

$$\tau(\lambda) = \begin{bmatrix} \cos(\kappa L) & -jsin(\kappa L) \\ -jsin(\kappa L) & \cos(\kappa L) \end{bmatrix} \quad (2.5)$$

Thus the sinusoidal distribution of P_b*(bar port)* and P_c*(cross port)* at $z = L_{DC}$ can be derived as [32]:

$$P_b(\lambda) = \cos^2(\kappa L_{DC}) \cdot P_{in}(\lambda) = |t|^2 P_{in}(\lambda) \quad (2.6a)$$

$$P_c(\lambda) = \sin^2(\kappa L_{DC}) \cdot P_{in}(\lambda) = |k|^2 P_{in}(\lambda) \quad (2.6b)$$

where the self coupling coefficient t and cross coupling coefficient k are defined as [38]:

$$t = \cos(\kappa L_{DC}) \quad \text{and} \quad k = e^{-j\pi/2} \sin(\kappa L_{DC}) \quad (2.7)$$

respectively. The term $e^{-j\pi/2}$ represents that the relative phase difference between field amplitudes. The term κ is the coupling strength, as given by:

$$\kappa(\lambda) = \frac{\beta_s(\lambda) - \beta_a(\lambda)}{2} = \frac{\pi \Delta n(\lambda)}{\lambda} \quad (2.8)$$

and $\Delta n(\lambda) = n^s_{eff}(\lambda) - n^a_{eff}(\lambda)$. (2.9)

At every successive L_c distance, power transfers completely from one port to other port, thus L_c is called cross coupling length or beat length. The 3-dB coupling length of DC can be estimated as:

$$L_{3dB}(\lambda) = \frac{L_{c(\lambda)}}{2} = \frac{(2m+1)\pi}{4\kappa(\lambda)} \quad (2.10)$$

where m = 0, 1, 2, 3. Thus for any coupling length, the power splitting ratio of a DC is highly wavelength dependent. In the following section, we will focus on the dispersion engineering of supermodes by varying waveguide design parameters(W,h).

2.2.2 Super mode Dispersion: Simulation Results

The wavelength dependent performance of a DC is better understood by calculating the dispersion characteristics of its supermodes.. The symmetric and anti-symmetric supermodes of a DC are evaluated numerically using Lumerical's Eigen mode Solver including the material dispersion parameters for core and cladding [29,30]. First simulations were done for Si platform based on the results of Ramesh K. Gupta's thesis [28] before moving on to Silicon Nitride platform and then the results of the two platforms are compared..We start with different DC cross sections (DC1, DC2 , DC3 and DC4) with fixed G and H respectively and with air cladding.

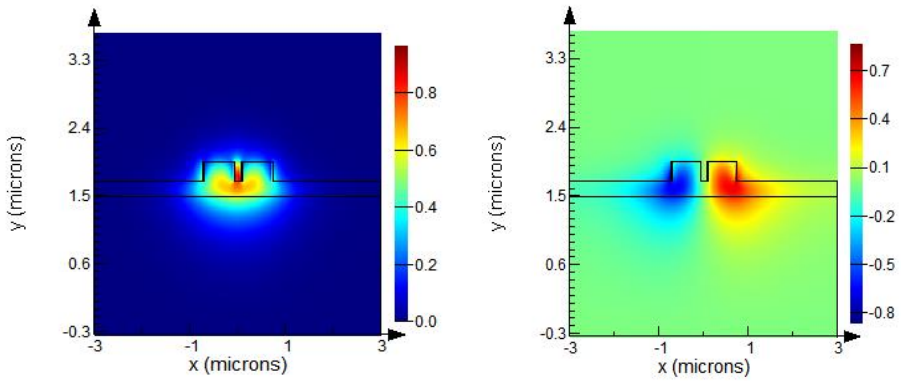

Figure 2.4: Electric field distribution(E_x) of TE-like (symmetric and antisymmetric) modes calculated for an operating wavelength λ = 1550 nm for a SiN on Insulator DC 1 with W=650 nm, h= 200nm, H= 450 nm, G=150 nm

As discussed earlier, the waveguide parameters (W , H, h) chosen for all the three DCs are such that they support only the fundamental modes (TE-like). However, because of wavelength dependent mode-field distributions, the waveguide modes as well as symmetric and anti-symmetric supermodes of the DCs are expected to be dispersive.

$$\Delta n_g(\lambda) = \Delta n(\lambda) - \lambda \frac{d}{d\lambda}[\Delta n(\lambda)] \quad (2.11)$$

is the differential group index of DC supermodes. If a DC is designed that $\Delta ng \rightarrow 0$ over a range of wavelength, it exhibits wavelength independent transmission characteristics within that band. . This is in fact similar to the design of zero differential group delay in multi-core fiber .It is also evident that values of $\Delta \mathbf{n(\lambda) = n^{s}_{eff} - n^{a}_{eff}}$ and the slope $\frac{\boldsymbol{d}}{\boldsymbol{d\lambda}}$ **([Δn(λ)])** of the DCs can be engineered appropriately by controlling the design parameters such as W, H, h, and G.

The free spectral range (FSR) of the transmitted light waves at both the output ports is given as:

$$\Delta\lambda = -\frac{\lambda^2}{L_{DC}\Delta n_g} \quad (2.12)$$

2.2.3 Condition for Wavelength Independent Coupling

A wavelength independent DC (WIDC) is characterized by $\Delta n_g(\lambda) \rightarrow 0$ (zero dispersion) for which FSR ($\Delta\lambda$) $\rightarrow \infty$. So we can write :-

$$\frac{d\kappa(\lambda)}{d\lambda} = -\frac{\pi}{\lambda^2}\,\Delta n_g(\lambda) \sim 0 \quad (2.13)$$

Hence the condition for a WIDC is as follows:

$$\boxed{\Delta n_g(\lambda) = 0 \Rightarrow \quad \kappa(\lambda) \text{constant for all } \lambda s} \quad (2.14)$$

This means that coupling strength κ is wavelength independent for any non-dispersive DC geometry over the entire range of operating wavelengths.

In order to find out the optimized WIDC geometries we first evaluated the geometry dependent values of Δn_g by varying the values of W and h (ensuring single-mode guidance in TE-like propagation at $\lambda \sim 1550$ nm), keeping constant values of $H = 220$ nm ,$G = 150$ nm for SOI case and H = 500 nm , G = 150 nm for SiN .

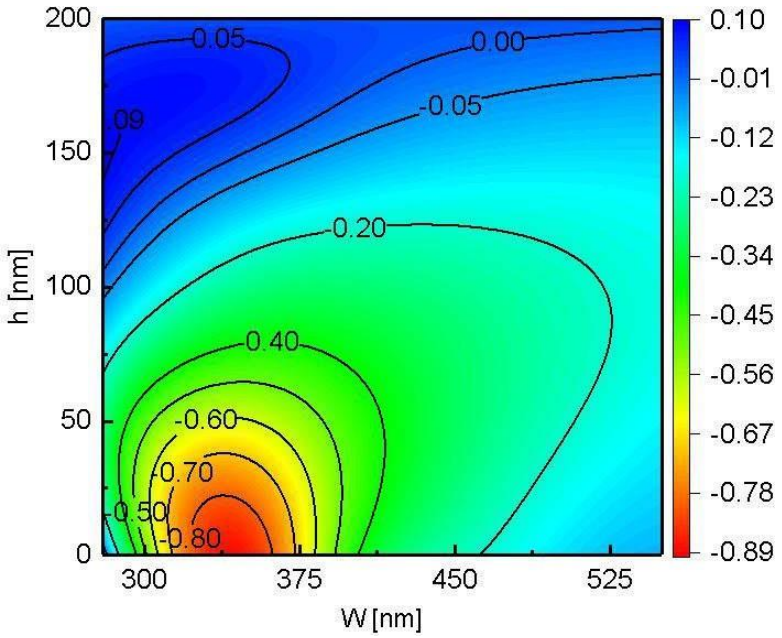

Figure 2.5: Contour plot of Δn_g in W - h plane calculated for H = 220 nm, G = 150 nm and TE polarization at λ = 1550 nm in SOI [28].

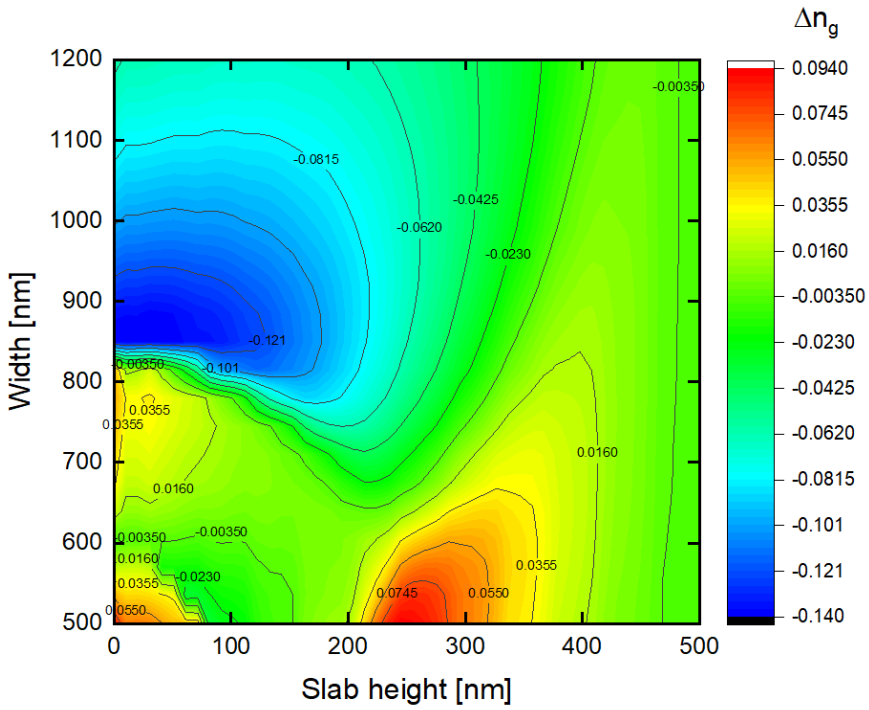

Figure 2.6: Contour plot of Δn_g in h-W plane calculated for H = 500 nm, G = 150 nm and TE polarization at λ = 1550 nm in SiN on Insulator.

Fig 2.5 and Fig 2.6 reveal that a DC can be indeed designed and fabricated with $\Delta n_g \rightarrow 0$ and $FSR \rightarrow \infty$.

Thus one can optimize the design parameters of a WIDC operating over a broad wavelength range for which Δn_g can be considered non-dispersive.

Also by comparing the plots, we notice that Δn_g *for* SiN shows less variation compared to Si for a wider range of widths, which concludes the less dispersive nature of nitride platform. Therefore width variation due to fabrication will not majorly affect the device characteristics.

Fig.2.7 shows that among the four designs, Δn_g variation for DC4 is relatively small, around zero within the given wavelength range(100 nm broadband) and it is likely to fulfill the design of a WIDC in SOI. Again, Δn_g is relatively large and highly dispersive for DC3 the design can be used for a wavelength dependent DC (WDDC). *The he value of $\kappa(\lambda)$ must remain constant over the wavelength range of interest for WIDC operation (DC4)* and it should be reasonably large for the sake of compact footprint of the device (lower value of L_{DC}).

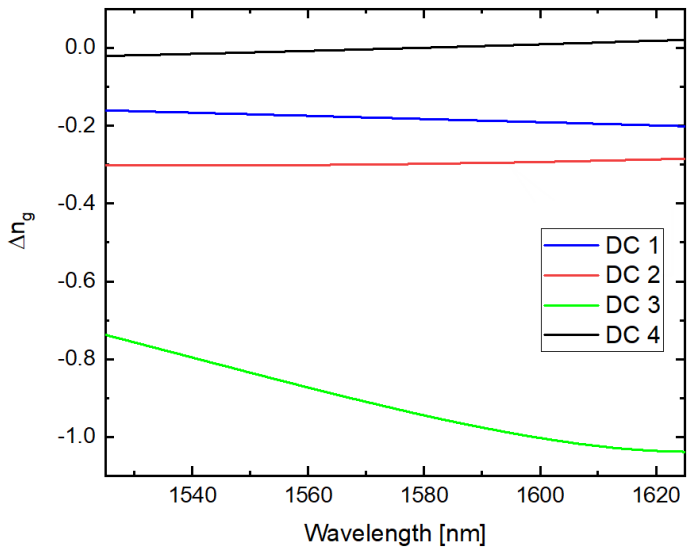

Figure 2.7: Calculated Δn_g as a function of wavelength for four different DC geometries: DC1 with W = 550 nm, h = 150 nm; DC2 with W = 350 nm, h = 100 nm; DC3 with W = 350 nm, h = 0 nm; and DC4 with W = 375 nm, h = 160 nm. In all cases H = 220 nm, G = 150 nm and calculated for TE-polarization in SOI with air cladding .

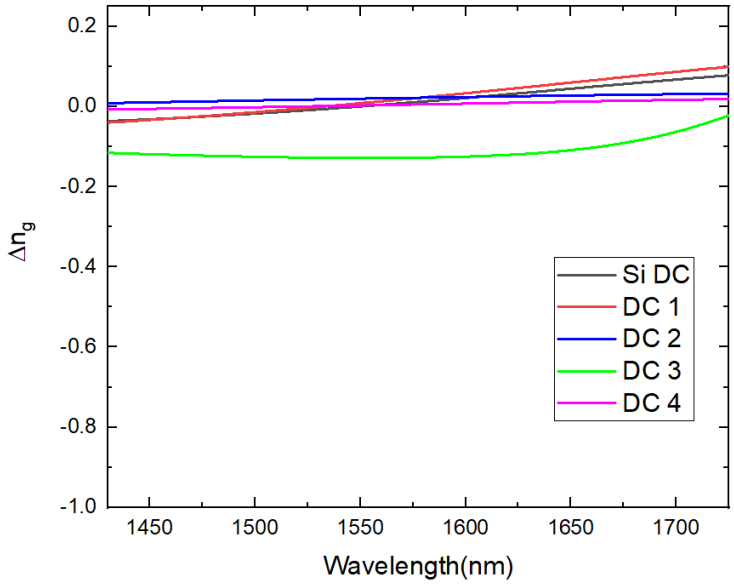

Figure 2.8: Calculated Δn_g *as* a function of wavelength in SiN on Insulator for four different DC geometries along with SOI DC : DC 1 with W = 650 nm, h = 200 nm; DC 2 with W = 850 nm, h = 350 nm; DC 3 with W = 850 nm, h =100 nm; and DC 4 with W = 1000 nm, h = 350 nm. In all cases H = 450 nm, G = 150 nm and calculated for TE-polarization in SiN with air cladding

Fig.2.8, Δn_g variation for DC 2 and DC 4 are relatively small, around zero within the given wavelength range (300 nm broadband) and they are likely to fulfill the design of a WIDC in SiN on Insulator . Again, Δn_g is relatively large and highly dispersive for DC 3; the design can be used for a wavelength dependent DC (WDDC) in SiN. The response of DC 1 is also fairly wavelength independent.

We observe that the response of SiN is better than Si for WIDC operation as DC 2 and DC 4 almost show negligible variation in Δn_g over the given wavelength range when compared to SOI DC (both with air cladding). Thus for wavelength independent operations over a wider bandwidth, we may alternatively choose the nitride platform.

It is worth mentioning that , although the contour plot was generated by fixing H at 500 nm , but we individually checked the device characteristics for each geometry separately by taking H= 450 nm and 500 nm for each of the six different DC designs. However only the optimized devices are mentioned in the thesis.

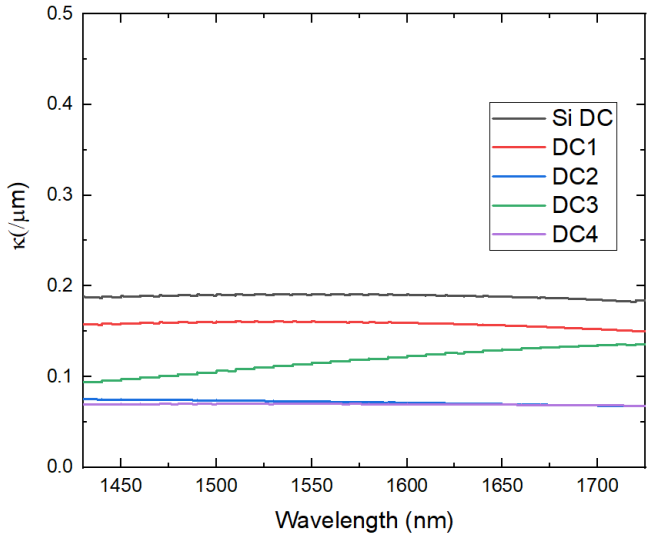

Figure 2.9: shows the estimated values $\kappa(\lambda)$ for all the above DC geometries . As expected, $\kappa(\lambda)$ is a strong function of λ for DC 3, whereas it is nearly wavelength independent for DC 1, DC 2 and DC 4 .

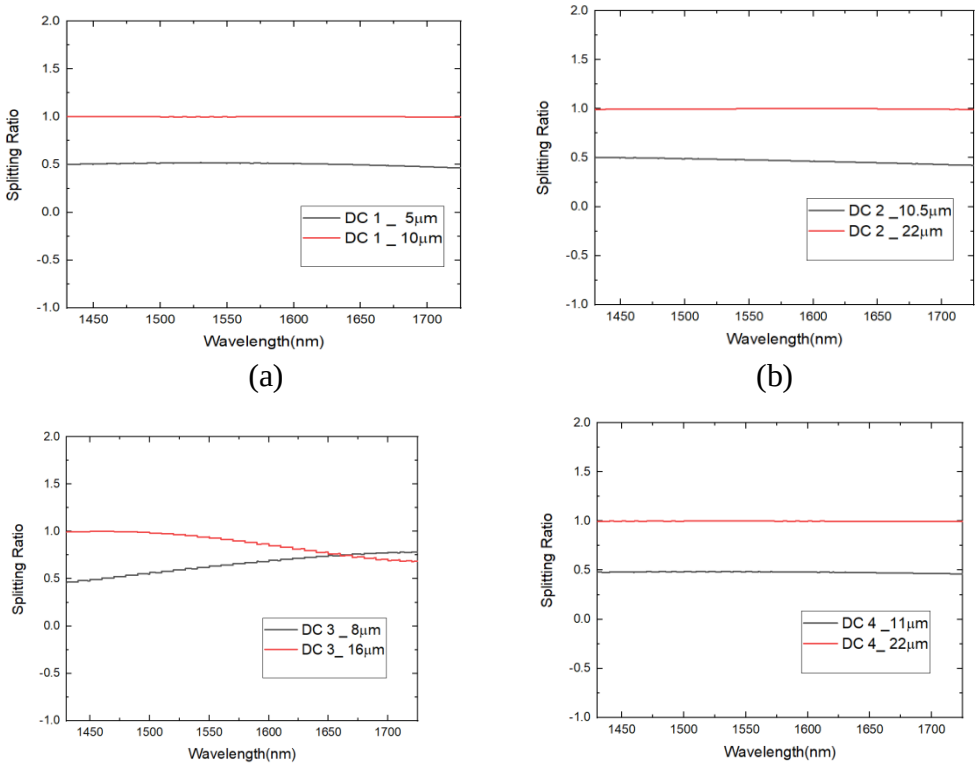

Figure 2.10: Power splitting ratios calculated at cross port (Pc/(Pc + Pb) as a function of wavelength for various DC designs showing L_{3dB} and Lc required for 50% and 100% coupling respectively .(a)DC 1 with W = 650 nm, h = 200 nm;(b) DC 2 with W = 850 nm, h = 350 nm;(c) DC 3 with W = 850 nm, h =100 nm; and(d) DC 4 with W = 1000 nm, h = 350 nm. In all cases H = 450 nm, G = 150 nm and calculated for TE-polarization in SiN with air cladding.

As expected DC 1, DC 2 and DC 4 designs (WIDCs) offer nearly wavelength independent transmission characteristics for all wavelengths from 1425nm-1725nm .DC1 has a lower foot print and higher value of κ and its 3-dB coupling length is 10 μm, which seems to be most efficient of all the designs considering all aspects. Although it may be more dispersive than DC 2 and DC 4 (Fig 2.8, owing to higher rib height in other two) but variation of Δn_g over given wavelength range is negligible. As κ is low in nitride (Fig 2.9) , so more L_{DC} is required in SiN compared to Si. Therefore, device footprint is increased.. On the other hand, the DC 3 design is highly wavelength dependent which may be useful for sensing applications.

2.3 Summary

We have formulated a simple design rule for a WIDC by solving the two propagating super-modes of a DC. The proposed WIDC design on nitride platform with air cladding and optimized waveguide parameters exhibits uniform coupling characteristics over a broad wavelength range in communication window (1425 nm ≤ λ ≤ 1725 nm) in TE-polarization. Broadband 2×2 WIDCs with various power splitting ratios were also demonstrated by varying L_{DC}. A compact WIDC design with deeply etched access waveguides can be demonstrated in future in a two step etching process. Thus SiN WIDCs can be suitably integrated in MRRs and MZIs to improve their optical bandwidth . Moreover it is now evident that SiN is definitely more tolerant to fabrication imposed width variations than Si.

CHAPTER 3

3. Conclusion

The major research outcomes of this thesis is the design and demonstration of a wavelength independent directional coupler (WIDC) with scalable power splitting ratios operating uniformly over a wide range of wavelengths in Silicon Nitride. This chapter presents a brief summary and outlook of the research work carried out in this thesis.

3.1 Thesis Summary

In summary, we have theoretically studied the coupling characteristics of a DC made of two single-mode waveguides in nitride platform and designed a WIDC with uniform coupling ratio over a broad wavelength range of nearly 300-nm near $\lambda = 1550$ nm in TE polarization. The fundamental design rule is to optimize the DC cross-sectional design parameters such as rib width (W), slab height (h), and gap (G) for which the coupling strength κ is nearly wavelength independent. In order to find out the optimized WIDC geometry we first calculated the geometry dependent values of differential group index of the supermodes ($\Delta n_g(\lambda) = n^s_g - n^{as}_g$) by varying the W and h (ensuring single mode guidance and TE-polarization) near $\lambda = 1550$ nm for fixed values of $H = 450\ nm$ and $G = 150$ nm. The coupling ratio and transmission characteristics of a typical WIDC ($W = 650$ nm and $h = 200$ nm) is found to be nearly wavelength independent (with lower footprint compared to other SiN DCs). The proposed WIDC can be fabricated on a 220-nm device layer SOI by etching out the Silicon and then depositing Silicon Nitride and then carrying out the required fabrication steps. In order to reduce the device footprint and to make the device more compact for MRRs and MZIs, a compact WIDC design with deeply etched access waveguides by selectively masking the shallow etched WIDC region in a two step fabrication process can be pursued.

REFERENCES

[1] C. Gunn *et al.*, "CMOS photonics for high-speed interconnects," *IEEE micro*, vol. 26, no. 2, pp. 58–66, 2006.

[2] Roel Baets et al ,"Silicon Photonics: silicon nitride versus silicon-on-insulator," OFC , OSA, 2016

[3] Daniel J Blumenthal et al, "Silicon Nitride in Silicon Photonics," Proceeding of IEEE, vol. 12, pp. 0018-9219 (2018).

[4] D.J. Moss et al, New CMOS-compatible platforms based on silicon nitride and Hydex for nonlinear optics. Nature Photonics 7, no. 8 (2013): 597-607.

[5] S. Miller et al, On-chip frequency comb generation at visible wavelengths via simultaneous second- and third-order optical nonlinearities, Optics Express, 22(22), p.26517-26525 (2014)

[6] A. S. Mayer et al, Frequency comb offset detection using supercontinuum generation in silicon nitride waveguides, Optics Express, 23(12), p.15440-15451 (2015)

[7] J. Khurgin et al, On the Origin of the Second-Order Nonlinearity in Strained Si-SiN Structures, arXiv: 1509.01166 (2015)

[8] W. M. Green, M. J. Rooks, L. Sekaric, and Y. A. Vlasov, "Ultra-compact, low RF power, 10 Gb/s silicon Mach-Zehnder modulator," *Optics Express*, vol. 15, no. 25, pp. 17 106–17113, 2007.

[9] D. Dai, J. Bauters, and J. E. Bowers, "Passive technologies for future large- scale photonic integrated circuits on silicon: polarization handling, light non-reciprocity and loss reduction," *Light: Science & Applications*, vol. 1, no. 3, p. e1, 2012.

[10] D. H. Lee, S. J. Choo, U. Jung, K. W. Lee, K. W. Kim, and J. H. Park, "Low-loss silicon waveguides with sidewall roughness reduction using a Sio_2 hard mask and fluorine-based dry etching," *Journal of Micromechanics and Microengineer- ing*, vol. 25, no. 1, p. 015003, 2014.

[11] J. F. Bauters, M. J. R. Heck, D. John, D. Dai, M. C. Tien, J. S. Barton, A. Leinse, R. G. Heideman, D. J. Blumenthal, and J.E. Bowers,"Ultra-low-loss high-aspect-ratio Si3N4 waveguides," Opt. Express 19, 3163–3174 (2011).

[12] M. C. Tien, J. F. Bauters, M. M. R. Heck, D. J. Blumenthal, and J. E. Bowers, "Ultra-low loss Si3N4 waveguides with low nonlinearity and high power handling capability," Opt. Express 18, 23562–23568 (2010).

[13] W. Bogaerts, P. De Heyn, T. Van Vaerenbergh, K. De Vos, S. Kumar Selvaraja,T. Claes, P. Dumon, P. Bienstman, D. Van Thourhout, and R. Baets, "Silicon microring resonators," *Laser & Photonics Reviews*, vol. 6, no. 1, pp. 47–73, 2012.

[14] P. Dumon, W. Bogaerts, V. Wiaux, J. Wouters, S. Beckx, J. Van Campenhout, D. Taillaert, B. Luyssaert, P. Bienstman, D. Van Thourhout et al., "Low-loss SOI photonic wires and ring resonators fabricated with deep uv lithography," IEEE Photonics Technology Letters, vol. 16, no. 5, pp. 1328–1330, 2004.

[15] G. R. Bhatt, R. Sharma, U. Karthik, and B. K. Das, "Dispersion-free SOI interleaver for DWDM applications," Journal of Lightwave Technology, vol. 30, no. 1, pp. 140–146, 2012.

[16] Z. Fang and C. Z. Zhao, "Recent progress in silicon photonics: a review," *ISRN Optics*, vol. 2012, 2012

[17] B. E. Saleh, M. C. Teich, and B. E. Saleh, *Fundamentals of photonics*. Wiley New York, 1991, vol. 22.

[18] J. Van Campenhout, W. M. Green, S. Assefa, and Y. A. Vlasov, "Low-power, 2x2 silicon electro-optic switch with 110-nm bandwidth for broadband reconfigurable optical networks," *Optics Express*, vol. 17, no. 26, pp. 24 020–24 029, 2009.

[19] K. Jinguji, N. Takato, A. Sugita, and M. Kawachi, "Mach-Zehnder interferometer type optical waveguide coupler with wavelength-flattened coupling ratio," *Electronics Letters*, vol. 26, no. 17, pp. 1326–1327, 1990.

[20] S.-L. Tsao, H.-C. Guo, and Y.-J. Chen, "Design of a 2 × 2 MMI MZI SOI electro-optic switch covering C band and L band," *Microwave and Optical Technology Letters*, vol. 33, no. 4, pp. 262–265, 2002.

[21] Z. Lu, H. Yun, Y. Wang, Z. Chen, F. Zhang, N. A. Jaeger, and L. Chrostowski, "Broadband silicon photonic directional coupler using asymmetric-waveguide based phase control," *Optics Express*, vol. 23, no. 3, pp. 3795–3808, 2015.

[22] R. Halir, A. Maese-Novo, A. Ortega-Moñux, I. Molina-Fernández,J. Wangüemert-Pérez, P. Cheben, D.-X. Xu, J. Schmid, and S. Janz, "Col- orless directional coupler with dispersion engineered sub-wavelength structure," *Optics Express*, vol. 20, no. 12, pp. 13 470–13 477, 2012.

[23] Y. Wang, Z. Lu, M. Ma, H. Yun, F. Zhang, N. A. Jaeger, and L. Chrostowski, "Compact broadband directional couplers using subwavelength gratings," *IEEE Photonics Journal*, vol. 8, no. 3, pp. 1–8, 2016.

[24] G. F. Chen, J. R. Ong, T. Y. Ang, S. T. Lim, C. E. Png, and D. T. Tan, "Broadband silicon-on-insulator directional couplers using a combination of straight and curved waveguide sections," *Scientific Reports*, vol. 7, no. 1, p. 7246, 2017.

[25] H. Morino, T. Maruyama, and K. Iiyama, "Reduction of wavelength dependence of coupling characteristics using si optical waveguide curved directional coupler," *Journal of Lightwave Technology*, vol. 32, no. 12, pp. 2188–2192, 2014.

[26] M. Alam, J. N. Caspers, J. S. Aitchison, and M. Mojahedi, "Compact low loss and broadband hybrid plasmonic directional coupler," Optics Express, vol. 21, no. 13, pp. 16 029–16 034, 2013.

[27] J. N. Caspers and M. Mojahedi, "Measurement of a compact colorless 3 db hybrid plasmonic directional coupler," Optics Letters, vol. 39, no. 11, pp. 3262– 3265, 2014.

[28] Ramesh K Gupta," Broadband Silicon Photonics Devices with Wavelength Independent Directional Couplers," ," Ph.D. dissertation, Indian Institute of Technology Madras, Chennai, 2019.

[29] "Lumerical MODE Solutions," www.lumerical.com.

[30] C. D. Salzberg and J. J. Villa, "Infrared refractive indexes of silicon germanium and modified selenium glass," JOSA, vol. 47, no. 3, pp. 244–246, 1957.

[31] A. Yariv and P. Yeh, Photonics: Optical electronics in modern communications (the Oxford series in electrical and computer engineering). Oxford University Press, Inc., 2006.

[32] W.-P. Huang, "Coupled-mode theory for optical waveguides: an overview," JOSA A, vol. 11, no. 3, pp. 963–983, 1994.